

Alma Mater Studiorum Università di Bologna  
Archivio istituzionale della ricerca

QM/MM Nonadiabatic Dynamics: The SHARC/COBRAMM Approach

This is the final peer-reviewed author's accepted manuscript (postprint) of the following publication:

*Published Version:*

Avagliano, D., Bonfanti, M., Garavelli, M., Gonzalez, L. (2021). QM/MM Nonadiabatic Dynamics: The SHARC/COBRAMM Approach. JOURNAL OF CHEMICAL THEORY AND COMPUTATION, 17(8), 4639-4647 [10.1021/acs.jctc.1c00318].

*Availability:*

This version is available at: <https://hdl.handle.net/11585/845935> since: 2022-01-17

*Published:*

DOI: <http://doi.org/10.1021/acs.jctc.1c00318>

*Terms of use:*

Some rights reserved. The terms and conditions for the reuse of this version of the manuscript are specified in the publishing policy. For all terms of use and more information see the publisher's website.

This item was downloaded from IRIS Università di Bologna (<https://cris.unibo.it/>).  
When citing, please refer to the published version.

(Article begins on next page)

# QM/MM Nonadiabatic Dynamics: The SHARC/COBRAMM Approach

*Davide Avagliano<sup>\*</sup> [a], Matteo Bonfanti<sup>†‡</sup> [b], Marco Garavelli<sup>[b]\*</sup>, Leticia González<sup>[a,c]\*</sup>*

<sup>[a]</sup>Institute of Theoretical Chemistry, Faculty of Chemistry, University of Vienna, Währinger Straße 17, A-1180 Vienna, Austria.

<sup>[b]</sup>

<sup>[c]</sup>Vienna Research Platform on Accelerating Photoreaction Discovery, University of Vienna, Währinger Straße 17, A-1180 Vienna, Austria.

## Corresponding Authors

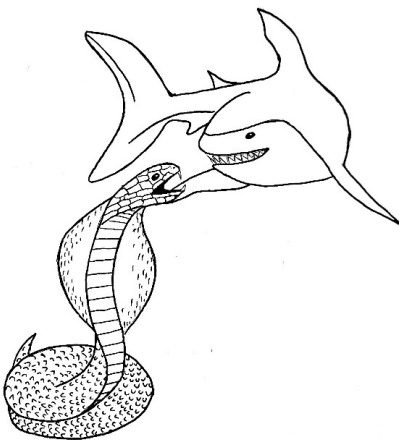
\*marco.garavelli@unibo.it; \*leticia.gonzalez@univie.ac.at

† Present address:

## ABSTRACT

We present the SHARC/COBRAMM approach to enable easy and efficient excited states dynamics simulations at different levels of electronic structure theory in the presence of complex environments using a quantum mechanics/molecular mechanics (QM/MM) setup. SHARC is a trajectory surface-hopping method that can incorporate the simultaneous effects of non-adiabatic and spin-orbit couplings in the excited state dynamics of molecular systems. COBRAMM allows ground and excited state QM/MM calculations using a subtractive scheme, with electrostatic embedding and a hydrogen link-atom approach. The combination of both free and open-source program packages provides a modular and extensive framework to model nonadiabatic processes after light irradiation from the atomistic to the nano-scale. As an example, the relaxation of acrolein from the  $S_1$  to  $T_1$  in solution is provided.

## TOC



**KEYWORDS** Nonadiabatic dynamics, QM/MM, internal conversion, intersystem crossing, SHARC, COBRAMM

## 1. INTRODUCTION

Nonradiative processes,<sup>1</sup> i.e. processes triggered by radiation in which no photons are emitted, are an integral feature of many chemical reactions initiated by light. These nonradiative transitions can be illustrated with a simple Jablonski energy diagram (see Figure 1a) and include relaxation within electronic states of the same spin multiplicity –the so-called internal conversion<sup>2</sup> (IC)— or between states with a change of spin multiplicity –coined as intersystem crossing<sup>3</sup> (ISC). Two aspects of these nonradiative phenomena are important to determine how a molecule relaxes after light irradiation: the time scale it takes to return to the electronic ground state and its nonadiabaticity, i.e. the degree of coupling existing between the electronically excited states in regions of degeneracy of the potential energy surfaces (PES).<sup>4</sup> Despite its apparent simplicity, to characterize these features is still a great challenge today, both from the experimental<sup>5</sup> and computational<sup>6</sup> points of view.

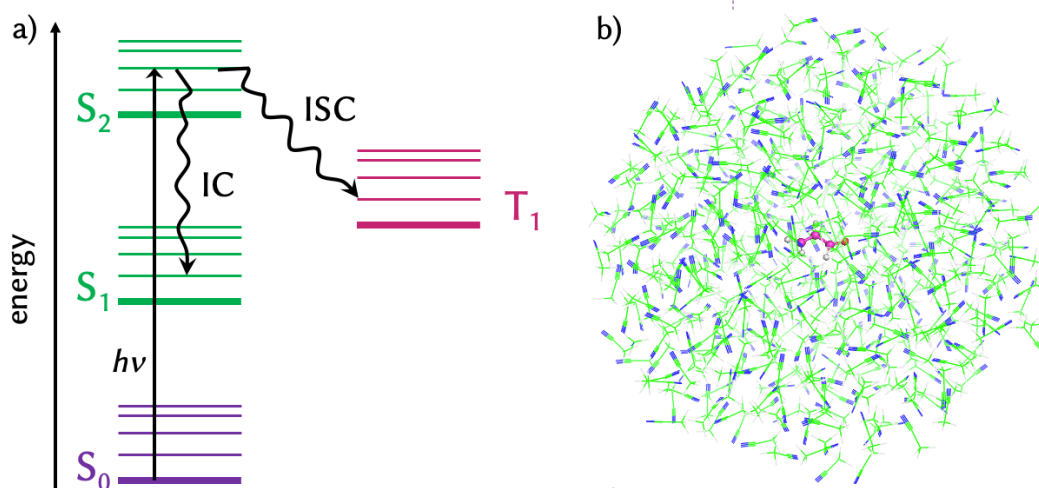


Figure 1: a) Jablonski energy diagram representing nonradiative processes that can occur after light absorption ( $h\nu$ ): internal conversion (IC) between states of same multiplicity and intersystem crossing (ISC) between states of different multiplicity. b) Example of QM/MM partition, with acrolein (QM part) surrounded by acetonitrile molecules (MM part).

A great variety of different methods have been developed to-date to simulate the time evolution of electronic excited states.<sup>7</sup> Methodologies based on a quantum description of both nuclear and

electronic degrees of freedoms<sup>8</sup> come at a very high computational cost and are not feasible for large-size molecules in their full multi-dimensional configuration space. Mixed quantum-classical methods,<sup>9</sup> where the nuclei follow classical equations of motion and the electrons are propagated based on quantum mechanics calculations, are a good trade-off between accuracy and computational feasibility. One of these methods is trajectory surface hopping<sup>10</sup> (TSH). There, an ensemble of independent trajectories is able to mimic a wavepacket propagation on different PES, allowing for 'hops' between them, subject to certain criteria. One big advantage of TSH is that it allows calculating all quantities needed to propagate the trajectories, i.e. electronic energies, gradients and nonadiabatic couplings, on-the-fly. Depending on the chosen electronic structure method, with their intrinsic advantages and limitations associated thereof, different levels of accuracy and computational efficiency can be achieved. And yet, even the cheapest (and most approximated) of the methods clashes with the dream of describing quantum mechanically the enormous number of degrees of freedom that are needed to include environmental effects surrounding the chromophore(s) of interest.<sup>11</sup> For such an endeavour, one often draws upon hybrid quantum mechanical/molecular mechanics (QM/MM) methodologies.<sup>12,13</sup> The virtue of the QM/MM approach is to divide the system in at least two layers that are treated at different levels of theory (see Figure 1b) –although schemes with more layers are also possible.<sup>14</sup> The chromophore is typically treated with a high-level quantum mechanical method, while the energy of its surrounding, biological or material environment or solvent molecules, can be approximated with parametrized potentials derived from force fields (FF). In this way, QM/MM allows treating systems otherwise intractable by either QM or MM.

In this work, we present a new approach to simulate nonadiabatic dynamics with TSH including the effect of the environment through a QM/MM partition. This approach is based on the

combination of the SHARC<sup>15,16,17</sup> (Surface Hopping including Arbitrary Couplings) and the COBRAMM<sup>18,19</sup> (Computations at Bologna Relating Ab-initio and Molecular Mechanics) methods. This marriage allows for a very efficient simulation of the time-evolution of excited states in complex environments.

In the next sections, we describe the essence of SHARC, the code that performs TSH including any kind of nonadiabatic couplings, and of COBRAMM, the code that obtains QM/MM ground and electronically excited states energies and gradients. This is followed by the nuts and bolts underlying the implementation of the SHARC/COBRAMM interface. Finally, we present an application of the photodynamics of acrolein in acetonitrile.

## **2. SHARC IN A NUTSHELL**

Introduced by Tully in 1971<sup>20</sup>, TSH is widely used due to its relatively simple formulation based on independent trajectories approximation, which makes the calculations easily parallelizable. Each nuclear classical trajectory of an ensemble is based on on-the-fly calculated electronically excited states PES. In order to include nonadiabaticity, the trajectories are allowed to stochastically change the active state in every step, by instantaneously hopping from one state to another. The hopping probability is calculated for each step based on the time-dependent expansion coefficient of the wavefunctions. These include the nonadiabatic coupling, as off-diagonal elements of diabatic Hamiltonian, and make hops more likely in regions of electronic degeneracy, where the nonadiabatic couplings are strongly localized. The prominent feature of SHARC<sup>16</sup> is the ability to include any arbitrary coupling in the propagation algorithm and thus to consider e.g. spin-orbit couplings to simulate ISC. As the choice of an active state is based on the electronic wavefunction, an essential part of SHARC approach is the choice of a suitable wavefunction representation. In a

QM calculation, the Hamiltonian calculated by most electronic structure codes contains only the molecular Coulomb interaction, and is therefore known as the molecular Coulomb Hamiltonian (MCH).<sup>21</sup> Relativistic effects, like spin-orbit couplings, or additional laser couplings, are not included in the MCH, but can be incorporated. The resulting, we call it “full” Hamiltonian, has eigenstates that correspond to the diagonal elements of the diagonalized MCH. Figure 2 represents graphically the eigenstates of the two representations obtained with few singlets and one triplet state.

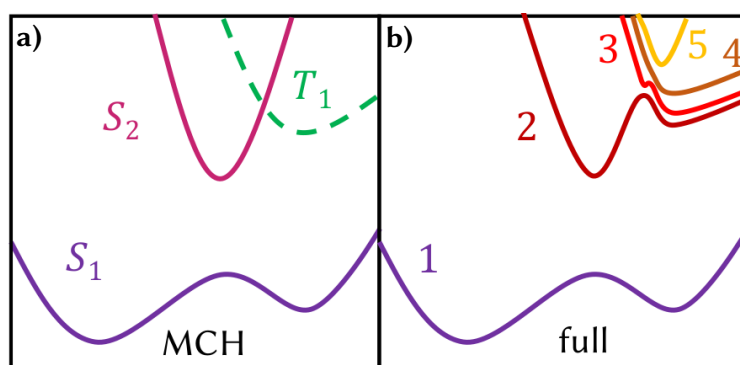


Figure 2: Example of wavefunction representations including two singlet and one triplet states. a) Eigenstates in the molecular Coulomb Hamiltonian (MCH) representation. Here, states are labelled according to their multiplicity. b) Eigenstates of the full representation. States are labelled according to their energetic order. Note that the triple is a multiplet with three states.

Ad hoc modifications to the propagation algorithm are employed in SHARC to obtain the wavefunction propagation in the full representation using the MCH data obtained from the QM codes,<sup>16</sup> i.e. to obtain the diagonal wavefunction coefficients from the MCH ones and calculate the hopping probabilities using them. Later, the gradient of the chosen state to be followed is calculated in the full representation, from the MCH gradients and nonadiabatic couplings. These modifications of the algorithm allow to get more accurate energies, localized couplings, and less hops between states of different multiplicity.<sup>16</sup>

### 3. COBRAMM IN A NUTSHELL

Introduced in 1976, the QM/MM methodology<sup>22</sup> opened the door to study complex chemical systems including large environmental effects.<sup>12</sup> The basic idea of QM/MM is to partition the full system in different parts that are then treated at different levels of theory. Accordingly, the energy of the total system is obtained combining the partial energy of the different components in a suitable form. COBRAMM<sup>18,19</sup> allows QM/MM electronic structures computation of molecules in their electronic ground and excited states. There exists different schemes to calculate the QM/MM energy, the one implemented in COBRAMM is called a subtractive scheme.<sup>12</sup> Assuming a standard QM/MM partition, first the QM energy relative to the QM part is calculated ( $E_{QM}$ ), then the energy of the total system is obtained at the FF level ( $E_{MM(tot)}$ ) and finally the energy of the QM part, but at MM level ( $E_{MM(QM)}$ ), is required to be subtracted from the total energy expression as,

$$E_{QM/MM} = E_{QM} + E_{MM(tot)} - E_{MM(QM)}$$

This scheme allows a straightforward generalization to more than two-layers, as it is implemented in the ONIOM-like scheme.<sup>23</sup> In COBRAMM, the system can be partitioned in up to three layers (Figure 3a). The first layer is treated at a QM high-level of theory; the second, medium layer, which is allowed to move during the dynamics, is represented at the MM level; and the third, low layer, also is described by energies computed at the MM level, but with a gradient set to zero and with their integrating molecules frozen during the dynamics. In principle, in the formulation of the energy within the subtractive scheme, the electrostatic interaction between regions is included and treated at the MM level, but that can be improved –as done in COBRAMM– in the framework of an electrostatic embedding scheme.<sup>24</sup> There, the MM point charges are incorporated in the QM Hamiltonian and the QM electron density is polarized by the MM part. Additionally, also the



contribution of the QM electronic density on the MM point charges gradient is considered when the MM atoms are propagated. The full interaction energy is finally completed by the Coulombic interaction between the regions, a van der Waals term, as parametrized in the force field chosen, and a correction for eventual covalent bonds that are cut by the QM/MM separation.

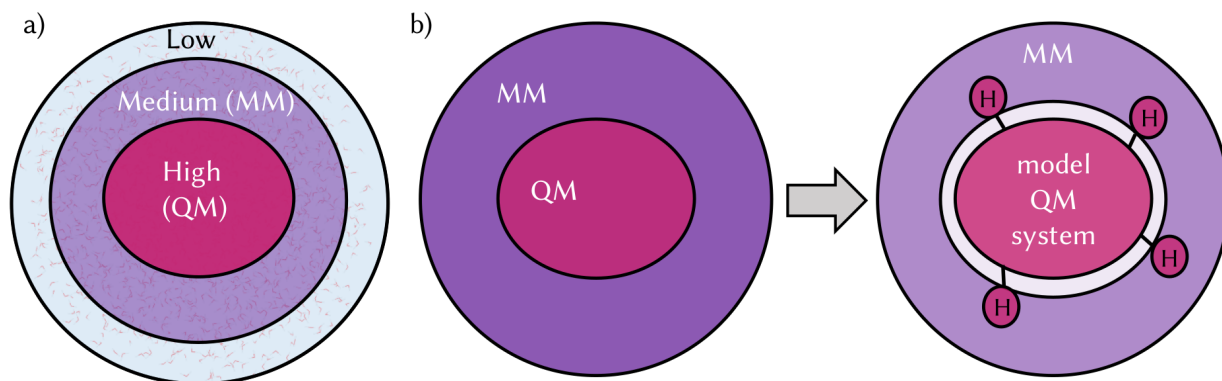


Figure 3: Graphical representation of the QM/MM scheme employed in COBRAMM; a) three layers partition; b) boundary region description with the link atom approach

Indeed, the latter is a delicate aspect that needs to be considered when the desired partition involves only part of a chromophore and consequently the boundary region between the QM and the MM part includes covalent bonds. This is usually handled with the link-atom approach<sup>12</sup> (Figure 3b). The covalent bond is cut and the QM-atom MM-atom covalent bond is substituted by a QM-atom and H atom bond, and the hydrogen atom is then included in the QM part. In order to avoid spurious effects, COBRAMM considers four important aspects to treat the boundary region: i) the MM charges need to be opportunely modified to avoid spurious electrostatic effects induced by the new atom; ii) the MM calculations do not include the new atom, which is defined in the topology file as a dummy atom without mass and charge; iii) the QM-H distance is constrained during the dynamics; and iv) the gradient of H is projected to the QM and MM adjacent atoms.

COBRAMM also comes with ad-hoc tools designed to facilitate, automatize and speed up the cumbersome time-consuming and often frustrating set-up of QM/MM calculations. It also includes its own interfaces to standard QM (Gaussian **PUR REF**, MOLCAS<sup>26</sup> and OpenMolcas<sup>27</sup>) and MM (AMBER<sup>25</sup>) software packages to allow QM/MM calculations. TSH (Tully based) schemes to allow nonadiabatic QM/MM dynamics at the RASSCF, RASPT2 and TDDFT levels, and tools for modelling the corresponding transient spectroscopies, are also present although these won't be employed in the current implementation that will rely on the SHARC schemes for both QM calculations, couplings and nonadiabatic dynamics.

## 4. IMPLEMENTATION OF THE SHARC/COBRAMM APPROACH

### 4.1 GENERAL WORKFLOW

The SHARC/COBRAMM approach is set to combine the main strengths of both software packages to carry out efficient QM/MM nonadiabatic molecular dynamics simulations. Before presenting the workflow, we shall introduce the six components (i-vi) of the two codes involved in the calculations that integrate the new software. The first two are the cores programs: (i) the executable Fortran90 program *sharc.x*, which is the core of the SHARC code and is in charge of running the dynamical propagation; and (ii) the Python program *cobramm.py*, which is the manager part of COBRAMM code in charge of the QM/MM partition and energy and gradient calculations. Additionally, both SHARC and COBRAMM codes rely on interfaces to external software to compute energy, gradients and couplings, and that requires two interfacing scripts: (iii) the interface of SHARC to a QM code, via the so-called Python *SHARC\_QM.py* interfaces, where QM stands for one of the available codes; and (iv) the interface of COBRAMM to AMBER<sup>25</sup> to

calculate MM energies and gradients, the Python script called *amberCalculator.py*. Additional information about the COBRAMM/AMBER interface can be found elsewhere.<sup>19</sup> Beyond these already available four blocks of the two codes, two new scripts were ad-hoc written to interface both softwares. The first is (v) a Python script *SHARC\_COBRAMM.py*, called by *sharc.x*, which connects both SHARC and COBRAMM codes: the script sets up the environments and the QM/MM calculation, it allows the communication between the two main codes in the different phases of the calculations, connecting their respective languages, and calls *cobram.py* from SHARC. The second (vi) is another Python script, *sharcQMcalculator.py*, which is called by COBRAMM and runs QM calculations using one of the available *SHARC\_QM.py* interfaces. In order to do that, it reads the original SHARC input, it rewrites it to calculate only energies and gradients of the QM part. Additionally, the script writes a point charges file to be read by the QM software to include the effect of the MM region and at the end of the QM calculations, the script reads the results and returns the output of the QM/MM calculation in SHARC format.

Now, we shall outline the general workflow of the SHARC/COBRAMM approach. In short, the SHARC suite performs the dynamical calculations, propagating wavefunctions and nuclei, while COBRAMM –through its interface to AMBER and calling the SHARC interfaces to the chosen electronic structure code – calculates the energies at the QM/MM level on-the-fly. In Figure 4 we shows the general workflow. Table 1 specifies which task is carried out by which program code.

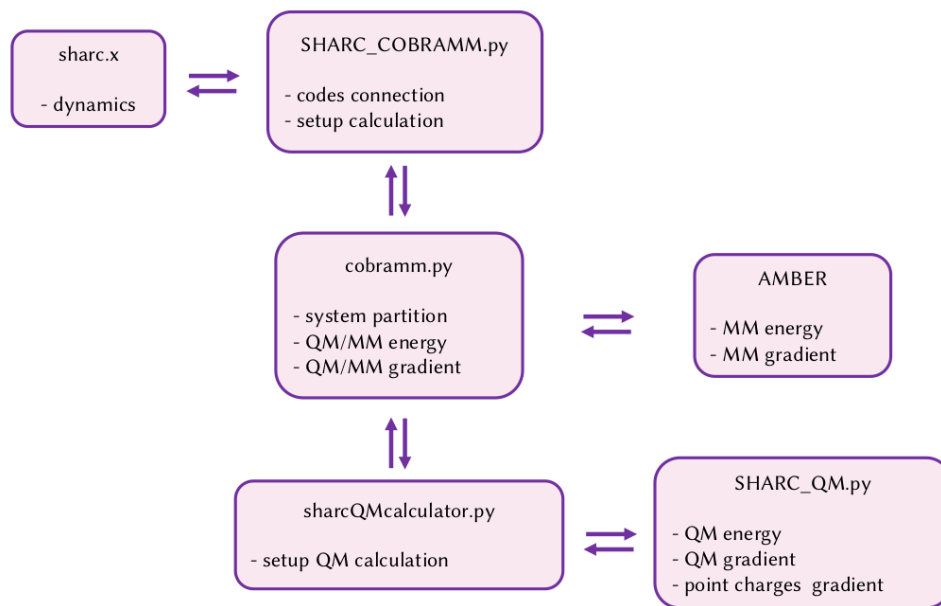


Figure 4: Schematic representation of SHARC/COBRAMM workflow

One should keep in mind that besides the two main codes (SHARC and COBRAMM), one requires suitable further software packages to obtain the MM and QM properties. The former is currently achieved in COBRAMM with AMBER. The QM energies, gradients and couplings can be provided with many QM packages, some of which are interfaced with SHARC.<sup>17</sup> Currently, the codes habilitated to work within SHARC/COBRAMM are: i) MOLCAS<sup>26</sup> and OpenMolcas,<sup>27</sup> to perform complete active space self-consistent field (CASSCF) and second order perturbation theory based on multiconfigurational self-consistent theory (CASPT2) calculations of energies, gradients and couplings (*SHARC\_MOLCAS.py*); ii) TURBOMOLE,<sup>28,29</sup> for electronic structure calculations at the algebraic diagrammatic construction (ADC) scheme of the polarization propagator level (*SHARC\_RICC2.py*);<sup>30</sup> and ii) ORCA,<sup>31</sup> for excited state dynamics at linear response time-dependent density functional theory (TD-DFT) level of theory (*SHARC\_ORCA.py*).<sup>32</sup> Additional information about *SHARC\_MOLCAS.py*, *SHARC\_RICC2.py* and *SHARC\_ORCA.py* interfaces can be found elsewhere.<sup>17</sup> Small modifications to each of these

three *SHARC\_QM.py* interfaces were required to include the reading of the point charges file and include those in the input file for the QM software, and to return the state specific point charges gradient induced by the QM electron density (see section S2 of the Supporting Information).

Table 1: Tasks partition in the SHARC/COBRAMM workflow

TASK	CODE
QM energy	QM software
MM energy	AMBER
QM/MM energy	<i>cobram.py</i> , called by <i>SHARC_COBRAMM.py</i>
QM gradient	QM software, called by <i>SHARC_QM.py</i> , called by <i>sharcQMcalculator.py</i>
MM gradient	AMBER
Point charges gradient	QM software
QM/MM gradient	<i>cobram.py</i> , called by <i>SHARC_COBRAMM.py</i>
Propagation	<i>sharc.x</i>

## 4.2 GENERATION OF INITIAL CONDITIONS

An important aspect of a TSH simulation is the generation of initial conditions. Based on the size and complexity of the system, there are different strategies to generate an accurate and appropriate ensemble of initial conditions.<sup>33,34,35</sup> Both SHARC and COBRAMM provide a series of auxiliary scripts to generate a proper set of initial conditions, listed in Table 2. Here we propose a protocol based on the combination of auxiliary scripts that are present in both SHARC and COBRAMM suites. The first step consists in generating an ensemble of initial geometries and velocities of the QM part, based on a ground state Wigner distribution.<sup>34,36</sup> Each of these geometries are solvated and then temperature and pressure of the solvent are equilibrated around the QM geometries. The

equilibration step is done with the MM code (AMBER) and the QM is kept frozen to not alter Wigner geometries and velocities. Once the equilibration is done, a droplet of solvent that embeds the QM part is cut for each of the geometries. At this point, a set of initial solvated geometries is obtained. Information about excited states for each of those and stochastic selection of the initial states can be done at this stage following the same procedure as implemented in SHARC.<sup>17</sup> This protocol was used for the generation of the initial conditions of acrolein –the application detailed in Section 5 (see also section S1 of the Supporting Information).

The combination of quantum and classical sets of geometries and velocities might in principle lead to very high oscillations in the energy during the first steps of the excited state simulation, as both the chromophore and the solvent are responding to the different level of theory the other part is treated. In that case and in order to avoid misbehaviors in the excited states dynamics due to this reason, we recommend to further equilibrate the system with QM/MM SHARC/COBRAMM dynamics in the electronic ground state. This leads to an excellent conservation, as expected for a TSH simulation, of the kinetic and total energy during the TSH dynamics (see Figure S2).

Table 2: Auxiliary scripts in SHARC and COBRAMM software helping initial condition generation and trajectories setup.

SCRIPT	TASK	SOFTWARE
wigner.py	calculate Wigner distribution of QM part	SHARC
cobramm-solvatedchromo.py	solvate the QM geometries	COBRAMM
cobramm-equilibration.py	equilibrate the MM part (AMBER)	COBRAMM
amber_to_initconds.py	convert AMBER to SHARC format	SHARC

combine_init.py	combine Wigner (QM) and classical (MM) velocities	SHARC
cobramm-droplet.py	Create solvent droplet and define high-medium-lower layers	COBRAMM
setup_cobramm_init.py	setup initial conditions excited states calculation	SHARC
excite.py	include excited states information for the initial geometries	SHARC
setup_cobramm_traj.py	Select initial states for the dynamics and setup the trajectories	SHARC

#### 4.3 POSITIONAL AND VELOCITY RESTRAINS OF SOLVENT ATOMS

Although not directly involved in the excited state dynamics, a wrong description of solvent molecules would alter the kinetic and total energy conservation of the full system,<sup>37</sup> possibly affecting the dynamics of the chromophore. This issue arises when, for example, rigid models are used to describe the potential energy where the solvent nuclei are propagated on, like the popular choice of TIP family of FF for water molecules.<sup>38</sup> When this FF are used, is good and common practice to impose positional and/or velocity constraints during a molecular dynamics runs, to avoid the high frequency motions of unphysical nature during the dynamics.<sup>39</sup> In SHARC the nuclei are propagated with the velocity-Verlet algorithm.<sup>40</sup> An iterative method proposed to correct positions and velocities along a trajectory based on this integration scheme is the so-called RATTLE algorithm<sup>41</sup>. We implemented RATLLE in *sharc.x* to be able to fix desired bond lengths during the dynamics. The implementations consists in two corrections that are applied at each step, to adjust first the distance and second the velocity, so that the bond length between the atoms is

kept constrained to an initial value defined by the user. This initial value is stored in a file that has to be provided by the user and can be generated manually or with an auxiliary script. We tested the implementation on a shell of 1500 TIP3P water molecules (MM) surrounding a SO<sub>2</sub> molecule (SHARC/COBRAMM/ORCA/AMBER, QM: B3LYP/def2-SVP) during a dynamical propagation of 400 fs. We prepared the system as explained in Section 4.2 and we ran twice an exemplary trajectory of SO<sub>2</sub> in water with the same initial condition and the same dynamics parameters, except for the positional and velocity restrain of the water molecules. As shown in Figure 5 the kinetic energy (Figure 5, top) of the system oscillates notably in case of unrestrained TIP3P dynamics in the first 200 fs. The oscillation period of the kinetic energy is reduced during the dynamics and goes to plateau, but the increases of kinetic energy leads to an increase of the temperature, calculated as  $T = 2KE/nk_b$ , where  $n$  is the number of degrees of freedoms of the moving part of the system, of almost 50K along the simulation time and KE the kinetic energy. This drastic increases and instability of kinetic energy reflects also in the total energy conservation (Figure 5, bottom), with oscillations of almost 1 eV in the first part of the dynamics. When RATTLE is applied to constrain the O-H distances of the TIP3P water molecules, the instability in KE disappears and the total energy of the full system is stable and conserved along the whole simulation time, as it should be. We therefore strongly recommend applying positional and velocity restrains when using approximate rigid models to calculate the potential energy of solvent molecules.



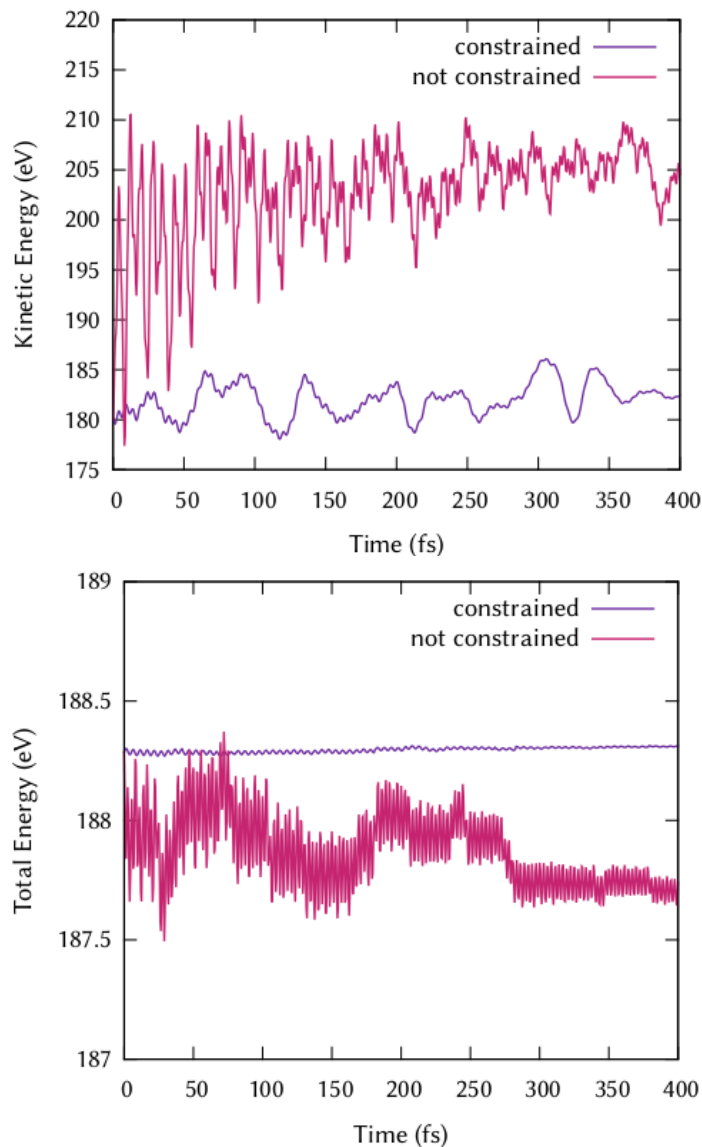


Figure 5: Kinetic (top) and total (bottom) energy along a  $\text{SO}_2/\text{H}_2\text{O}$  excited states SHARC/COBRAMM trajectory propagated with (purple) and without (pink) the RATTLE algorithm to constrain the O-H bond distances of TIP3P water molecules. The positional and velocity constrain avoids artificial increases of kinetic energy and instantaneous temperature of the system, thus allowing for conservation of the total energy of the system.

#### 4.4 SOLVENT ATOMS MASKING

The application of TSH on molecular systems also forces the user to choose among several options developed to rescale the kinetic energy after a hop,<sup>42</sup> to reflect a trajectory after a classically

forbidden hop (also known as frustrated hop)<sup>43</sup> or to impose decoherence corrections.<sup>44</sup> Kinetic energy rescaling is employed to preserve the total energy of the system after an instantaneous hop, which induces a change of potential energy. When the hopping probability algorithm indicates a hop, but the system does not contain enough energy to perform this so-called frustrated hop, there is the possibility to reflect the velocity vectors, keeping the trajectory in the same active state.<sup>45</sup> A decoherence correction is applied in TSH to avoid the lack of internal consistency.<sup>46</sup> This can be explained imagining a trajectory in state 2, where the coefficient of state 1 is still large, but the population of this state would still follow the gradient of the active state, which is different from the one of this state. Different correction schemes<sup>47,48,49,50</sup> have been implemented to allow only the population of state 2 to follow the gradient of state 2.

These three procedures regard only the QM part and thus the PES on which the wavefunction is propagated since hops between excited PES only occur on the chromophore part –solvent rearrangement effects occur in longer time scales. That means it is fundamental to restrict these adjustments in the TSH procedure only to the active part of the system in the excited states dynamics, the QM part, excluding the MM atoms, which otherwise would lead to artificial effects. We refer here to this procedure as atom masking. Rescaling the kinetic energy after a hop and reflecting the trajectory after a frustrated hop can be done parallel to the nonadiabatic coupling vector. In this case, the scheme would be size-consistent and atom masking is not necessary. However, if the nonadiabatic coupling vectors are not computed during the dynamics, the rescaling and reflection are often done isotropically, i.e. parallel to the velocity vector. In these schemes, it is important to include only the QM part in the rescaling and thus, atom masking is necessary. Regarding the decoherence correction, in the case of the commonly used energy based decoherence correction,<sup>46</sup> the coefficient of the inactive state is dampened based on the energy

difference between the states as well as the kinetic energy. Consequently, it is important to apply the atom masking to only consider the kinetic energy of the QM region only. Masking the MM can be done in the trajectory preparation steps thanks to the auxiliary scripts *setup\_cobramm\_traj.py*.

## **5. APPLICATION OF SHARC/COBRAMM TO ACROLEIN RELAXATION IN ACETRONITRILE**

In this section, we apply the SHARC/COBRAMM approach to carry out exemplary QM/MM nonadiabatic dynamics simulation on acrolein solvated in MeCN. Acrolein has been widely studied in the past as a model system to understand the photochemical behavior of enones.<sup>51,52</sup> In particular, after irradiation at 193 nm and relaxation to the  $S_1$  state, a dissociative pathway passing through the  $T_1$  was demonstrated in acetonitrile.<sup>53</sup> This pathway was proposed by static calculations in gas phase<sup>54</sup> and confirmed by previous TSH simulations<sup>55</sup> that evidenced ultrafast ISC within 500 fs.

The first step before running QM/MM TSH molecular dynamics is to obtain an ensemble of initial conditions. The QM part includes only the acrolein chromophore and the MM part included 500 MeCN molecules –half in the medium layer and half in the low layer— treated with the General Amber Force Field (GAFF).<sup>57</sup> We calculated 250 geometries from a Wigner distribution, based on frequencies at the optimized geometry of acrolein in gas phase. Those geometries were solvated with 1000 MeCN molecules using the Packmol software.<sup>58</sup> Each of these systems was minimized, heated at 300K, and equilibrated in volume and pressure, following a protocol detailed in Section S1 of the Supporting Information. After equilibration, a droplet of 500 MeCN molecules surrounding the centred acrolein was created for each of the initial systems. Each of these 250

systems was used to propagate ground state dynamics at the SHARC/COBRAMM//MOLCAS/AMBER level of theory during 250 fs to equilibrate the velocities of the system. As explained above, this step is necessary because the initial velocities for the QM part came from a Wigner distribution, while from the MM derives from classical force field dynamics. By doing this QM/MM dynamical simulation in the ground state, artificial increase of the kinetic energy to equilibrate the QM and MM parts is prevented. From the ensemble of ground state trajectories, we selected the last snapshot of 146 of those and excited them vertically to the  $S_1$ , from where they were propagated during 500 fs.

The so-prepared 46 trajectories were then initialized in the  $S_1$  state, including two electronic singlet and two triplet states. The acrolein chromophore is described at the CASSCF(8,7)/cc-pVDZ level of theory. The orbitals included in the active space are depicted in Fig. S1. The electronic structure calculations of the energies, gradients, and spin-orbit couplings were performed with OpenMolcas.<sup>27</sup> Nonadiabatic coupling were approximated computing wavefunction overlaps.<sup>56</sup> The electronic decoherence correction scheme was applied.<sup>46</sup>

In order to meaningfully compare our results to that available in the literature for acrolein in MeCN,<sup>55</sup> we purposely ran a statistically similar number of trajectories at the same level of theory, we included the same number of states and same active space, we solvated the chromophore with an analogue shell of solvent molecules, and we split the solvent molecules in mobile and frozen in a comparable way. We do not expect major differences coming from the fact that the two simulations employed different software packages for the QM, MM and dynamics calculations. However, here we generated the initial conditions following a different protocol than in Ref. 55 and used the “full” representation of SHARC for the TSH dynamics. We thus expect comparable

qualitative behaviour, but anticipate deviations in the relative populations and in the time constant for the  $S_1$  decay and the ISC.

Two pathways were identified<sup>55</sup> to populate  $T_1$  from the  $S_1$ . The first one is the result from initial ISC from  $S_1$  to  $T_2$ , which according to the El-Sayed's rule<sup>59</sup> is expected to be the most favourable decay channel, since  $S_1$  has a  $n\pi^*$  character and  $T_2$  a  $\pi\pi^*$  character<sup>54</sup>. After the population of  $T_2$ , an ultrafast IC to  $T_1$  is expected. The second pathway is due to the fact that  $T_1$  can acquire  $\pi\pi^*$  character during the dynamics and its proximity in energy to the  $S_1$  can make direct population likely. Additionally, an IC from the  $S_1$  to the ground state was also observed as a minor decay channel.

Our averaged state population analysis for the ensemble of trajectories (Figure 6a) shows an initial decay from  $S_1$  via ISC to  $T_2$ , in agreement with the El-Sayed's rule, from which the system quickly evolves to  $T_1$ . Along the dynamics only seven trajectories decay directly from  $S_1$  to  $T_1$ , whereas 34 trajectories prefer ISC to  $T_2$  followed by ultrafast IC between the two triplets, which represent the main contribution of the almost 30% of the final population (Figure 6a). The ground state is populated by IC from  $S_1$ , with only one trajectory of direct ISC from  $T_1$  to  $S_0$  and none to repopulate  $S_1$  with backward ISC. We fitted the population data and obtained a kinetic model for the relaxation from  $S_1$  and the population of  $T_1$  and  $S_0$  (Figure 6b). The full decay from  $S_0$  occurs in a picosecond time scale, both via ISC and population of  $S_0$  through IC. The model confirms the ultrafast time scale of the IC between the two triplets, with  $T_2$  relaxing to  $T_1$  after ca. 50 fs. The  $T_2$  state is populated via ISC due to symmetry reasons and acts as a doorway on the way to the lower energy  $T_1$  –in agreement with the involvement of  $T_1$  in the main reactive channel for acrolein in acetonitrile.<sup>53</sup>

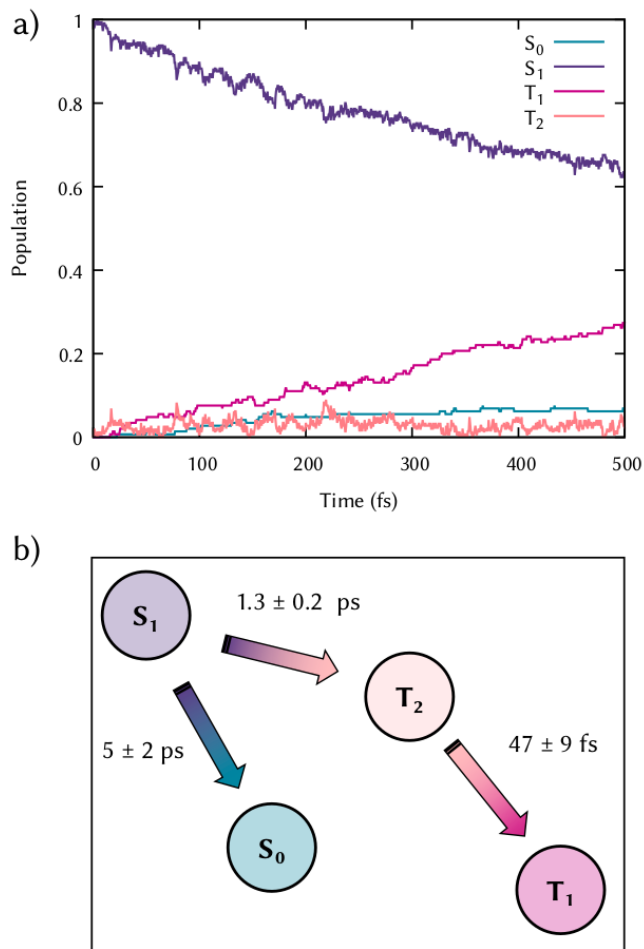


Figure 6: QM/MM nonadiabatic TSH dynamics of acrolein in acetonitrile: a) Time-resolved population averaged over 148 trajectories; b) kinetic model for the decay from  $S_1$  via internal conversion to  $S_0$  and intersystem crossing to  $T_2$  followed by ultrafast internal conversion to  $T_1$ .

## VI. CONCLUSIONS

We report an interface between SHARC and COBRAMM codes to simulate nonadiabatic dynamics with TSH method in complex environment with a mixed quantum/classical formalism for the calculation of the electronic energies. Combining the robust features of the two codes, this interface represents an efficient methodology to simulate excited states dynamics, including different type of potential couplings and environmental effects. While SHARC can describe efficiently ISC, COBRAMM can handle big size system or solvent effects on photodynamics of

chromophores due to energy partition and interfaces to external programs. Together, they allow to describe excited states dynamics at different level of theory for the quantum part of the system, including CASSCF and CASPT2, ADC and TD-DFT levels, including the powerful functionalities of AMBER suite for the classical part.

The applicability of this new tool was demonstrated on the study of acrolein in MeCN, which shows ISC from the singlet to the triple manifold as well as IC in the singlet manifold. We expect studies of chromophores in more complex biological environments to be the subject of future studies.

## ASSOCIATED CONTENT

### **Supporting Information:**

## AUTHOR INFORMATION

### **Author Contributions**

The manuscript was written through contributions of all authors. All authors have given approval to the final version of the manuscript. ‡D.A. and M.B. contributed equally.

## ACKNOWLEDGMENT

The authors thank funding from the European Union's Horizon 2020 research and innovation program under the Marie Skłodowska-Curie grant agreement No.765266 (LightDyNAMics) and

the H2020-NMBP-TO-IND-2018-2020/DT-NMBP-09-2018 grant agreement No. 814492 (SIMDOME). The Vienna Scientific Cluster is acknowledged for generous computational support.

## REFERENCES

- (1) Kasha, M. Characterization of Electronic Transitions in Complex Molecules. *Discuss. Faraday Soc.* **1950**, 9 (0), 14–19. <https://doi.org/10.1039/DF9500900014>.
- (2) Conical Intersections. *Advanced Series in Physical Chemistry*. WORLD SCIENTIFIC July 1, 2004, p 856. <https://doi.org/doi:10.1142/5406>.
- (3) Marian, C. M. Spin–Orbit Coupling and Intersystem Crossing in Molecules. *WIREs Comput. Mol. Sci.* **2012**, 2 (2), 187–203. <https://doi.org/https://doi.org/10.1002/wcms.83>.
- (4) Bernardi, F.; Olivucci, M.; Robb, M. A. Potential Energy Surface Crossings in Organic Photochemistry. *Chem. Soc. Rev.* **1996**, 25 (5), 321–328. <https://doi.org/10.1039/CS9962500321>.
- (5) Conti, I.; Cerullo, G.; Nenov, A.; Garavelli, M. Ultrafast Spectroscopy of Photoactive Molecular Systems from First Principles: Where We Stand Today and Where We Are Going. *J. Am. Chem. Soc.* **2020**, 142 (38), 16117–16139. <https://doi.org/10.1021/jacs.0c04952>.
- (6) Mai, S.; González, L. Molecular Photochemistry: Recent Developments in Theory. *Angew. Chemie Int. Ed.* **2020**, 59 (39), 16832–16846. <https://doi.org/https://doi.org/10.1002/anie.201916381>.
- (7) González, L.; Lindh, R. *Quantum Chemistry and Dynamics of Excited States: Methods*



*and Applications*; Wiley Online Books; 2020.

<https://doi.org/https://doi.org/10.1002/9781119417774>.

- (8) Curchod, B. F. E.; Martínez, T. J. Ab Initio Nonadiabatic Quantum Molecular Dynamics. *Chem. Rev.* **2018**, *118* (7), 3305–3336. <https://doi.org/10.1021/acs.chemrev.7b00423>.
- (9) Crespo-Otero, R.; Barbatti, M. Recent Advances and Perspectives on Nonadiabatic Mixed Quantum–Classical Dynamics. *Chem. Rev.* **2018**, *118* (15), 7026–7068. <https://doi.org/10.1021/acs.chemrev.7b00577>.
- (10) Barbatti, M. Nonadiabatic Dynamics with Trajectory Surface Hopping Method. *WIREs Comput. Mol. Sci.* **2011**, *1* (4), 620–633. <https://doi.org/https://doi.org/10.1002/wcms.64>.
- (11) Segatta, F.; Cupellini, L.; Garavelli, M.; Mennucci, B. Quantum Chemical Modeling of the Photoinduced Activity of Multichromophoric Biosystems. *Chem. Rev.* **2019**, *119* (16), 9361–9380. <https://doi.org/10.1021/acs.chemrev.9b00135>.
- (12) Senn, H. M.; Thiel, W. QM/MM Methods for Biomolecular Systems. *Angew. Chemie Int. Ed.* **2009**, *48* (7), 1198–1229. <https://doi.org/https://doi.org/10.1002/anie.200802019>.
- (13) Field, M. J.; Bash, P. A.; Karplus, M. A Combined Quantum Mechanical and Molecular Mechanical Potential for Molecular Dynamics Simulations. *J. Comput. Chem.* **1990**. <https://doi.org/10.1002/jcc.540110605>.
- (14) Nogueira, J. J.; Roßbach, S.; Ochsenfeld, C.; González, L. Effect of DNA Environment on Electronically Excited States of Methylene Blue Evaluated by a Three-Layered QM/QM/MM ONIOM Scheme. *J. Chem. Theory Comput.* **2018**.

<https://doi.org/10.1021/acs.jctc.8b00185>.

- (15) Richter, M.; Marquetand, P.; González-Vázquez, J.; Sola, I.; González, L. SHARC: Ab Initio Molecular Dynamics with Surface Hopping in the Adiabatic Representation Including Arbitrary Couplings. *J. Chem. Theory Comput.* **2011**.  
<https://doi.org/10.1021/ct1007394>.
- (16) Mai, S.; Marquetand, P.; González, L. Nonadiabatic Dynamics: The SHARC Approach. *WIREs Comput. Mol. Sci.* **2018**, 8 (6), e1370.  
<https://doi.org/https://doi.org/10.1002/wcms.1370>.
- (17) S. Mai, M. Richter, M. Heindl, M. F. S. J. Menger, A. J. A.; M. Ruckebauer, F. Plasser, L. M. Ibele, S. Kropf, M. Oppel, P. M.; González, L. SHARC2.1: Surface Hopping Including Arbitrary Couplings – Program Package for Non-Adiabatic Dynamics. Sharcm.org. 2019.
- (18) Altoè, P.; Stenta, M.; Bottoni, A.; Garavelli, M. A Tunable QM/MM Approach to Chemical Reactivity, Structure and Physico-Chemical Properties Prediction. *Theor. Chem. Acc.* **2007**, 118 (1), 219–240. <https://doi.org/10.1007/s00214-007-0275-9>.
- (19) Weingart, O.; Nenov, A.; Altoè, P.; Rivalta, I.; Segarra-Martí, J.; Dokukina, I.; Garavelli, M. COBRAMM 2.0 — A Software Interface for Tailoring Molecular Electronic Structure Calculations and Running Nanoscale (QM/MM) Simulations. *J. Mol. Model.* **2018**.  
<https://doi.org/10.1007/s00894-018-3769-6>.
- (20) Tully, J. C.; Preston, R. K. Trajectory Surface Hopping Approach to Nonadiabatic Molecular Collisions: The Reaction of H<sup>+</sup> with D<sub>2</sub>. *J. Chem. Phys.* **1971**, 55 (2), 562–572.

<https://doi.org/10.1063/1.1675788>.

- (21) Mai, S.; Marquetand, P.; González, L. A General Method to Describe Intersystem Crossing Dynamics in Trajectory Surface Hopping. *Int. J. Quantum Chem.* **2015**, *115* (18), 1215–1231. <https://doi.org/https://doi.org/10.1002/qua.24891>.
- (22) Warshel, A.; Levitt, M. Theoretical Studies of Enzymic Reactions: Dielectric, Electrostatic and Steric Stabilization of the Carbonium Ion in the Reaction of Lysozyme. *J. Mol. Biol.* **1976**, *103* (2), 227–249. [https://doi.org/https://doi.org/10.1016/0022-2836\(76\)90311-9](https://doi.org/https://doi.org/10.1016/0022-2836(76)90311-9).
- (23) Chung, L. W.; Sameera, W. M. C.; Ramozzi, R.; Page, A. J.; Hatanaka, M.; Petrova, G. P.; Harris, T. V; Li, X.; Ke, Z.; Liu, F.; Li, H.-B.; Ding, L.; Morokuma, K. The ONIOM Method and Its Applications. *Chem. Rev.* **2015**, *115* (12), 5678–5796. <https://doi.org/10.1021/cr5004419>.
- (24) Dohn, A. O. Multiscale Electrostatic Embedding Simulations for Modeling Structure and Dynamics of Molecules in Solution: A Tutorial Review. *Int. J. Quantum Chem.* **2020**, *120* (21), e26343. <https://doi.org/https://doi.org/10.1002/qua.26343>.
- (25) Salomon-Ferrer, R.; Case, D. A.; Walker, R. C. An Overview of the Amber Biomolecular Simulation Package. *WIREs Comput. Mol. Sci.* **2013**, *3* (2), 198–210. <https://doi.org/https://doi.org/10.1002/wcms.1121>.
- (26) Karlström, G.; Lindh, R.; Malmqvist, P.-Å.; Roos, B. O.; Ryde, U.; Veryazov, V.; Widmark, P.-O.; Cossi, M.; Schimmelpfennig, B.; Neogrady, P.; Seijo, L. MOLCAS: A Program Package for Computational Chemistry. *Comput. Mater. Sci.* **2003**, *28* (2), 222–

239. [https://doi.org/https://doi.org/10.1016/S0927-0256\(03\)00109-5](https://doi.org/https://doi.org/10.1016/S0927-0256(03)00109-5).
- (27) Fdez. Galván, I.; Vacher, M.; Alavi, A.; Angeli, C.; Aquilante, F.; Autschbach, J.; Bao, J. J.; Bokarev, S. I.; Bogdanov, N. A.; Carlson, R. K.; Chibotaru, L. F.; Creutzberg, J.; Dattani, N.; Delcey, M. G.; Dong, S. S.; Dreuw, A.; Freitag, L.; Frutos, L. M.; Gagliardi, L.; Gendron, F.; Giussani, A.; González, L.; Grell, G.; Guo, M.; Hoyer, C. E.; Johansson, M.; Keller, S.; Knecht, S.; Kovačević, G.; Källman, E.; Li Manni, G.; Lundberg, M.; Ma, Y.; Mai, S.; Malhado, J. P.; Malmqvist, P. Å.; Marquetand, P.; Mewes, S. A.; Norell, J.; Olivucci, M.; Oppel, M.; Phung, Q. M.; Pierloot, K.; Plasser, F.; Reiher, M.; Sand, A. M.; Schapiro, I.; Sharma, P.; Stein, C. J.; Sørensen, L. K.; Truhlar, D. G.; Ugandi, M.; Ungur, L.; Valentini, A.; Vancoillie, S.; Veryazov, V.; Weser, O.; Wesołowski, T. A.; Widmark, P.-O.; Wouters, S.; Zech, A.; Zobel, J. P.; Lindh, R. OpenMolcas: From Source Code to Insight. *J. Chem. Theory Comput.* **2019**, *15* (11), 5925–5964. <https://doi.org/10.1021/acs.jctc.9b00532>.
- (28) Furche, F.; Ahlrichs, R.; Hättig, C.; Klopper, W.; Sierka, M.; Weigend, F. Turbomole. *Wiley Interdiscip. Rev. Comput. Mol. Sci.* **2014**. <https://doi.org/10.1002/wcms.1162>.
- (29) Mai, S.; Plasser, F.; Pabst, M.; Neese, F.; Köhn, A.; González, L. Surface Hopping Dynamics Including Intersystem Crossing Using the Algebraic Diagrammatic Construction Method. *J. Chem. Phys.* **2017**, *147* (18), 184109. <https://doi.org/10.1063/1.4999687>.
- (30) Dreuw, A.; Wormit, M. The Algebraic Diagrammatic Construction Scheme for the Polarization Propagator for the Calculation of Excited States. *WIREs Comput. Mol. Sci.* **2015**, *5* (1), 82–95. <https://doi.org/https://doi.org/10.1002/wcms.1206>.

- (31) Neese, F. Software Update: The ORCA Program System, Version 4.0. *Wiley Interdiscip. Rev. Comput. Mol. Sci.* **2018**. <https://doi.org/10.1002/wcms.1327>.
- (32) Casida, M. E.; Huix-Rotllant, M. Progress in Time-Dependent Density-Functional Theory. *Annu. Rev. Phys. Chem.* **2012**, 63 (1), 287–323. <https://doi.org/10.1146/annurev-physchem-032511-143803>.
- (33) Nogueira, J. J.; González, L. Computational Photophysics in the Presence of an Environment. *Annu. Rev. Phys. Chem.* **2018**, 69 (1), 473–497. <https://doi.org/10.1146/annurev-physchem-050317-021013>.
- (34) Barbatti, M.; Sen, K. Effects of Different Initial Condition Samplings on Photodynamics and Spectrum of Pyrrole. *Int. J. Quantum Chem.* **2016**, 116 (10), 762–771. <https://doi.org/https://doi.org/10.1002/qua.25049>.
- (35) Mai, S.; Gattuso, H.; Monari, A.; González, L. Novel Molecular-Dynamics-Based Protocols for Phase Space Sampling in Complex Systems . *Frontiers in Chemistry* . 2018, p 495.
- (36) Dahl, J. P.; Springborg, M. The Morse Oscillator in Position Space, Momentum Space, and Phase Space. *J. Chem. Phys.* **1988**, 88 (7), 4535–4547. <https://doi.org/10.1063/1.453761>.
- (37) Weingart, O. Combined Quantum and Molecular Mechanics (QM/MM) Approaches to Simulate Ultrafast Photodynamics in Biological Systems. *Current Organic Chemistry*. 2017, pp 586–601. <https://doi.org/http://dx.doi.org/10.2174/1385272821666161108150421>.

- (38) Jorgensen, W. L.; Chandrasekhar, J.; Madura, J. D.; Impey, R. W.; Klein, M. L. Comparison of Simple Potential Functions for Simulating Liquid Water. *J. Chem. Phys.* **1983**, 79 (2), 926–935. <https://doi.org/10.1063/1.445869>.
- (39) Kräutler, V.; van Gunsteren, W. F.; Hünenberger, P. H. A Fast SHAKE Algorithm to Solve Distance Constraint Equations for Small Molecules in Molecular Dynamics Simulations. *J. Comput. Chem.* **2001**, 22 (5), 501–508. [https://doi.org/https://doi.org/10.1002/1096-987X\(20010415\)22:5<501::AID-JCC1021>3.0.CO;2-V](https://doi.org/https://doi.org/10.1002/1096-987X(20010415)22:5<501::AID-JCC1021>3.0.CO;2-V).
- (40) Swope, W. C.; Andersen, H. C.; Berens, P. H.; Wilson, K. R. A Computer Simulation Method for the Calculation of Equilibrium Constants for the Formation of Physical Clusters of Molecules: Application to Small Water Clusters. *J. Chem. Phys.* **1982**, 76 (1), 637–649. <https://doi.org/10.1063/1.442716>.
- (41) Andersen, H. C. Rattle: A “Velocity” Version of the Shake Algorithm for Molecular Dynamics Calculations. *J. Comput. Phys.* **1983**, 52 (1), 24–34. [https://doi.org/https://doi.org/10.1016/0021-9991\(83\)90014-1](https://doi.org/https://doi.org/10.1016/0021-9991(83)90014-1).
- (42) Jasper, A. W.; Hack, M. D.; Truhlar, D. G. The Treatment of Classically Forbidden Electronic Transitions in Semiclassical Trajectory Surface Hopping Calculations. *J. Chem. Phys.* **2001**, 115 (4), 1804–1816. <https://doi.org/10.1063/1.1377891>.
- (43) Jasper, A. W.; Truhlar, D. G. Improved Treatment of Momentum at Classically Forbidden Electronic Transitions in Trajectory Surface Hopping Calculations. *Chem. Phys. Lett.* **2003**, 369 (1), 60–67. [https://doi.org/https://doi.org/10.1016/S0009-2614\(02\)01990-5](https://doi.org/https://doi.org/10.1016/S0009-2614(02)01990-5).

- (44) Bittner, E. R.; Rossky, P. J. Quantum Decoherence in Mixed Quantum-classical Systems: Nonadiabatic Processes. *J. Chem. Phys.* **1995**, *103* (18), 8130–8143. <https://doi.org/10.1063/1.470177>.
- (45) Tully, J. C. Molecular Dynamics with Electronic Transitions. *J. Chem. Phys.* **1990**, *93* (2), 1061–1071. <https://doi.org/10.1063/1.459170>.
- (46) Granucci, G.; Persico, M. Critical Appraisal of the Fewest Switches Algorithm for Surface Hopping. *J. Chem. Phys.* **2007**, *126* (13), 134114. <https://doi.org/10.1063/1.2715585>.
- (47) Jain, A.; Alguire, E.; Subotnik, J. E. An Efficient, Augmented Surface Hopping Algorithm That Includes Decoherence for Use in Large-Scale Simulations. *J. Chem. Theory Comput.* **2016**, *12* (11), 5256–5268. <https://doi.org/10.1021/acs.jctc.6b00673>.
- (48) Granucci, G.; Persico, M.; Zocante, A. Including Quantum Decoherence in Surface Hopping. *J. Chem. Phys.* **2010**, *133* (13), 134111. <https://doi.org/10.1063/1.3489004>.
- (49) Subotnik, J. E.; Shenvi, N. A New Approach to Decoherence and Momentum Rescaling in the Surface Hopping Algorithm. *J. Chem. Phys.* **2011**, *134* (2), 24105. <https://doi.org/10.1063/1.3506779>.
- (50) Jaeger, H. M.; Fischer, S.; Prezhdo, O. V. Decoherence-Induced Surface Hopping. *J. Chem. Phys.* **2012**, *137* (22), 22A545. <https://doi.org/10.1063/1.4757100>.
- (51) Wilsey, S.; González, L.; Robb, M. A.; Houk, K. N. Ground- and Excited-State Surfaces for the [2+2]-Photocycloaddition of  $\alpha,\beta$ -Enones to Alkenes. *J. Am. Chem. Soc.* **2000**, *122* (24), 5866–5876. <https://doi.org/10.1021/ja0006595>.

- (52) Reguero, M.; Olivucci, M.; Bernardi, F.; Robb, M. A. Excited-State Potential Surface Crossings in Acrolein: A Model for Understanding the Photochemistry and Photophysics of .Alpha.,.Beta.-Enones. *J. Am. Chem. Soc.* **1994**, *116* (5), 2103–2114. <https://doi.org/10.1021/ja00084a056>.
- (53) Wu, W.; Yang, C.; Zhao, H.; Liu, K.; Su, H. Photodissociation and Photoisomerization Dynamics of CH<sub>2</sub>=CHCHO in Solution. *J. Chem. Phys.* **2010**, *132* (12), 124510. <https://doi.org/10.1063/1.3352421>.
- (54) Fang, W.-H. A CASSCF Study on Photodissociation of Acrolein in the Gas Phase. *J. Am. Chem. Soc.* **1999**, *121* (36), 8376–8384. <https://doi.org/10.1021/ja982334i>.
- (55) Cui, G.; Thiel, W. Generalized Trajectory Surface-Hopping Method for Internal Conversion and Intersystem Crossing. *J. Chem. Phys.* **2014**, *141* (12), 124101. <https://doi.org/10.1063/1.4894849>.
- (56) Plasser, F.; Ruckebauer, M.; Mai, S.; Oppel, M.; Marquetand, P.; González, L. Efficient and Flexible Computation of Many-Electron Wave Function Overlaps. *J. Chem. Theory Comput.* **2016**, *12* (3), 1207–1219. <https://doi.org/10.1021/acs.jctc.5b01148>.
- (57) Wang, J.; Wolf, R. M.; Caldwell, J. W.; Kollman, P. A.; Case, D. A. Development and Testing of a General Amber Force Field. *J. Comput. Chem.* **2004**, *25* (9), 1157–1174. <https://doi.org/https://doi.org/10.1002/jcc.20035>.
- (58) Martínez, L.; Andrade, R.; Birgin, E. G.; Martínez, J. M. PACKMOL: A Package for Building Initial Configurations for Molecular Dynamics Simulations. *J. Comput. Chem.* **2009**, *30* (13), 2157–2164. <https://doi.org/https://doi.org/10.1002/jcc.21224>.



- (59) El-Sayed, M. A. Triplet State. Its Radiative and Nonradiative Properties. *Acc. Chem. Res.* **1968**, *1* (1), 8–16. <https://doi.org/10.1021/ar50001a002>.